Investigation of the morphological, optical and antimicrobial properties of Nd doped ZnO nanoparticles using *Hemidesmus indicus (L.) R. Br.* Root extracts

M. Karthikeyan*[1], A. Manohar[1], P. Vijaya Kumar[2], A. Jafar Ahamed[3], A. Ravikumar[4], A. Vinoth[1] and M. Priyadharshan[1]

[1]Department of Chemistry, Periyar Maniammai Institute of Science and Technology, Vallam, Thanjavur- 613 403, Tamil Nadu, India.
[2]Department of Chemistry, Jairams Arts and Science College, Affiliated to Bharathidasan University, Karur- 639 003 Tamil Nadu, India.
[3]Post Graduate and Research Department of Chemistry, Jamal Mohamed College (Autonomous), Affiliated to Bharathidasan University, Tiruchirappalli - 620 020, Tamil Nadu, India.
[4]Department of Chemistry, SRM TRP Engineering College, Tiruchirappalli, Tamil Nadu – 621 105

Corresponding Author E-mail: karthichemist10@gmail.com

Abstract:

In the current study, we present a low-cost, novel, and straightforward method for the biopreparation of zinc oxide nanoparticles (ZnO NPs) and neodymium (Nd^{3+}) incorporated into the ZnO NPs using extracts of *Hemidesmus indicus* (*H. indicus*) (L.) R. Br. root like a sustainable reducing as well as coating agent. Rietveld's analysis of the XRD data showed that ZnO and Nd^{3+} doped ZnO NPs have a hexagonal wurtzite crystalline level. The morphological representation of synthesized NPs was analyzed by FESEM and chemical composition by EDAX. The different vibrational frequencies were assigned for the FT-IR spectra. The Optical behaviour of the prepared NPs be present studies by UV–visible spectroscopy. Moreover, this study concludes the antimicrobial efficiency of the synthesized NPs opposed to standard and clinical strains of *Staphylococcus aureus* (gram-positive) and *Klebsiella pneumoniae* (gram-negative) bacterial strains using the well diffusion method.

Keywords: ZnO, *Hemidesmus indicus*, antimicrobial activity.

1. Introduction

With its utilization in science and technology to create novel materials at the nanoscale, nanotechnology is developing as a quickly growing area [1]. ZnO-NPs have advantageous in a variety of fields, including optical, magnetic and gas sensing. The fact that they have a high catalytic efficiency, a strong adsorption capacity, a moderate isoelectric point and have rapid ion transport kinetics for biosensing may also be helpful. ZnO is frequently employed as a substitute for TiO_2 in photodegradation mechanisms. Due to its faster reaction rates, more active sites, and more efficiency at producing hydrogen peroxide, it has the highest photocatalytic activity [2].

These are widely used in the water purification process [3] to remove contaminants like arsenic and Sulphur [4]. ZnO-NPs are three versatile elements with a range of biological characteristics, such as antimicrobial [5] and antibacterial activity [6]. These are also employed in the creation of cosmetics in addition to the dental industry's usage of eugenol [7, 8], in bio molecular detection, diagnostics, antimicrobial textile industries, and microelectronics [5]. Furthermore, a lot of researchers have recently obtained ZnO NPs made from plant components [9–15].

Hemidesmus indicus (L.) R. Br., a part of the *Asclepiadaceae* family, is also known commercially as Indian Sarasaparilla, Nannari and Sariva and is commonly used in traditional Indian medicine. A wide range of applications for using the root extract like twining shrub, semi-erect shrub, slender, sometimes prostrate or laticiferous, which treating disorders like biliousness, diarrhea, blood diseases, skin diseases, respiratory disorders, syphilis, bronchitis, fever, rheumatism, and burning sensation. [16, 17]. According to phytochemistry studies, H. indicus includes flavonoids, volatile oils, triterpenes, coumarin, hemidesmine, hemidesmol, hemidesterol, stearoptin, pregnane glycosides, and saponins. [17, 18].

The biosynthesis of ZnO NPs was used by the aqueous root extract of *H. indicus*, there is no data was received from the literature survey regarding the biogenesis of Zinc oxide and metal-doped ZnO NPs using *H. indicus*. In the current study, we concentrated on the environmentally friendly reduction and stabilization of ZnO and Nd^{3+} doped ZnO NPs utilizing root extracts of *H. indicus.* The morphological, optical, and antimicrobial properties of as-produced NPs have been studied.

2. Preparation of ZnO and Nd^{3+} doped ZnO NPs using *H. indicus* root extract:

To prepare ZnO NPs, 10 g of *H. indicus* roots were rinsed several times Double-distilled (DD) water. These roots were boiled in a beaker with 100 mL of DD H_2O for an hour at 80°C. The root extract was filtered using Whatman filter paper. 0.1 M Zn $(NO_3)_2$. $6H_2O$ solution was used to dissolve 120 mL of *H. indicus* root extract.

The uniformly mixed nitrate solution was constantly stirred for 5 h at 80ºC. The output was the formation of the precipitate, which dried for 1 h at 110 °C. The as-prepared ZnO NPs were heated at 600°C for 4 h. Additionally, to synthesize Nd^{3+} doped ZnO NPs,

0.002 M Neodymium (III) nitrate hydrate ($Nd(NO_3)_3.6H_2O$) were mixed to 0.098 M Zinc Nitrate Hexahydrate ($Zn(NO_3)_2.6H_2O$), which was subsequently dissolved in 120 ml of *H. indicus* root extracts. Finally, the mixture was continuously stirred at 80°C for 5 h. The Nd^{3+} doped ZnO NPs was calcined at 700°C for 5h. Fig. 1 displays the schematic diagram of prepared ZnO as well as Nd^{3+} doped ZnO NPs using *H. indicus root* extracts.

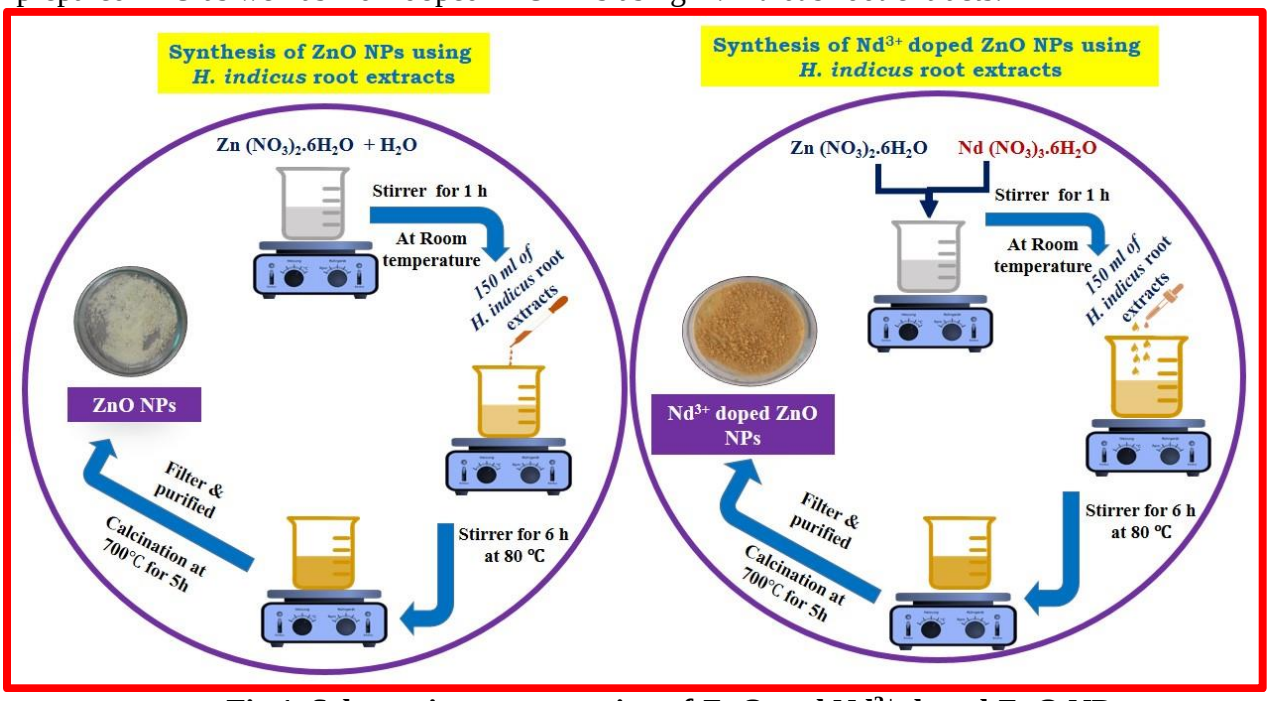

Fig 1. Schematic representation of ZnO and Nd^{3+} doped ZnO NPs

2.2 Microbiological Study

Using the well diffusion method, the antibacterial activity of ZnO and Nd^{3+} doped ZnO NPs against *Staphylococcus aureus* and *Klebsiella pneumoniae* were investigated. The needed quantity of NPs was combined with 1.5 mg/ml of dimethyl sulphoxide to test the antibacterial activity. The prepared material had been incubated at 37°C for an overnight period prior to this phase, and the zone of inhibition measurements (mm) were determined after one day. The antibiotic amoxicillin was employed as a positive control.

2.3. Material Characterizations

Fourier Transform Infrared Spectrometer, the structural properties of synthesized using Perkin-Elmer. X-ray diffraction (XRD) analyze was studied using Rigaku D/Max-2400 diffractometer. Gemini 300 (Carl Zeiss) instrument was used to examine the samples' surface properties and compositional analyses. With the use of a PerkinElmer Lambda 35 UV-vis spectrometer, the UV-visible spectrum was captured.

3. Results and Discussion

3.1. XRD analysis

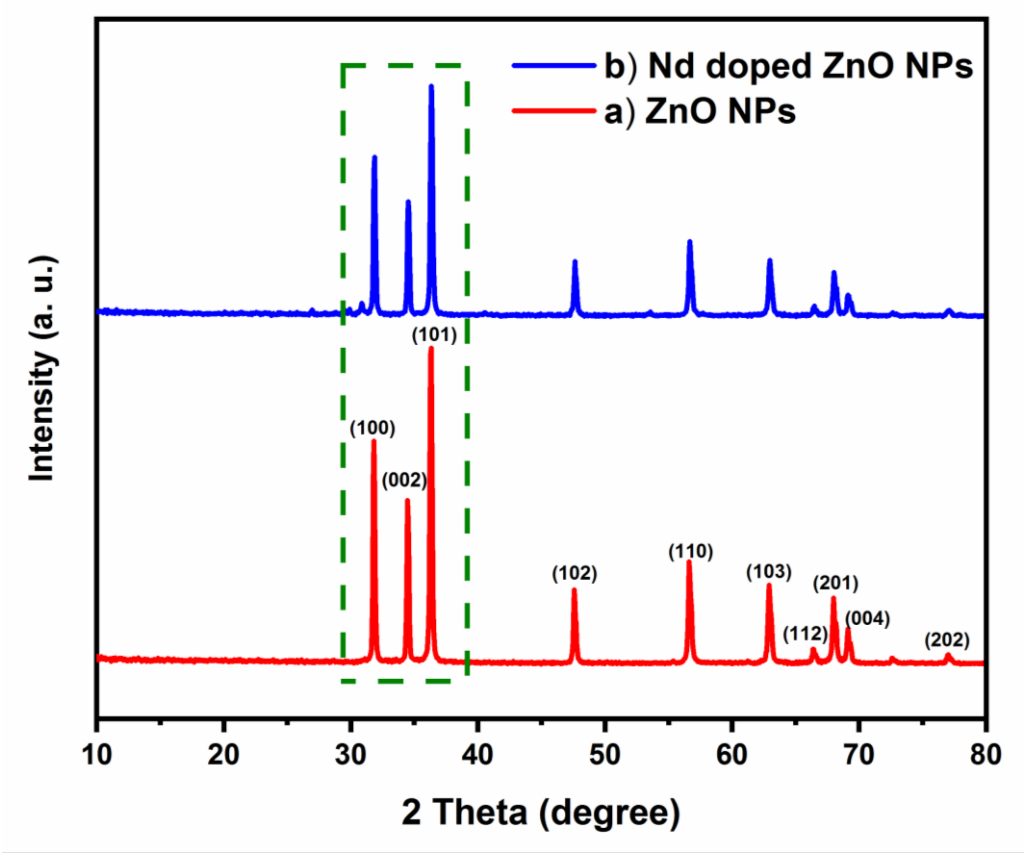

Fig. 2. XRD patterns of a) ZnO NPs b) Nd^{3+} doped ZnO NPs

The X-ray diffraction (XRD) patterns of the synthesized samples were shown in Fig.2. The detected diffraction peaks closely match the value provided on JCPDS card no. 36-1451. The prepared samples exhibited the hexagonal wurtzite phase without any impurities. Additionally, it is evident that the intensity peak of the Nd^{3+} doped ZnO NPs decreased when compared to ZnO. The Nd^{3+} doping seems to have substantially modified the crystalline nature of ZnO NPs on the decrease in the sharpness of the diffraction peaks in the Nd^{3+} doped ZnO. In addition, we have noted the significant intensity decreased in the peak position of 31.86, 34.53 and 36.35, which was confirms the doping element of Nd^{3+} on the surface ZnO. In addition to this result, we also observe the Nd^{3+} doped ZnO NPs XRD peak broadening, which shows that they are smaller in size than pure ZnO NPs. The introduction of impurities allows a host ZnO lattice to distort, which may create the crystallite size to decrease. The presence of Nd^{3+} also slows the nucleation and subsequent growth rate of ZnO NPs. Further analysis of the XRD spectra showed that in the Nd^{3+} doped ZnO NPs, some XRD peaks that appeared in pure ZnO NPs at higher angles disappeared.

This occurs as a result of a reduction in grain size and the presence of strain in the ZnO lattice caused by the entry of the Nd3+ dopant atom into the host ZnO matrix. As a result, we draw the conclusion that a slight change in the 2 values of the diffraction peaks and a broadening of the peak are attributable to an increase in micro-strain, and that the size and micro-strain of doped ZnO NPs mostly contribute to the line broadening effect. The size reduction of Nd^{3+} doped ZnO NPs is notable when compared to pure ZnO NPs, as seen in Table 1.

Figure 2 clearly demonstrates how Nd^{3+} doping causes the features peak to migrate toward greater 2θ angle values. The fact that the peak positions have changed so significantly reveals that the Nd^{3+} ions in the Zn^{2+} position of ZnO crystal lattice have been fully incorporated [19]. Also, the Debye Scherrer equation (Eq.1) can be used to determine the average particle size. It was determined to be about 49 and 42 nm for pure ZnO NPs and Nd^{3+} doped ZnO NPs and this information is shown in Table 1.

$$D = \frac{k\lambda}{\beta \cos\theta} \quad \text{---------- (1)}$$

Where λ, k and β - is the wavelength of the radiation, constant (0.94) and the peak width at half-maximum in radians. As shown in Table 1, was proved clearly that, in comparison to pure ZnO NPs, lattice strain and dislocation density rise with Nd^{3+} ion doping. The calculated lattice constants of "a" and "c" from the d spacing values using Eq. (2), and their values are displayed in Table 1.

$$\frac{1}{d^2} = \frac{4}{3}\left(\frac{h^2+hk+k^2}{a^2}\right) + \frac{l^2}{c^2} \quad \text{---------- (2)}$$

For the doped element Nd^{3+}, the ionic radius value is 0.995, while for Zn^{2+}, it is 0.74. Table 1 shows that the value of the lattice parameters and the d value are clearly decreasing as a result of the larger ionic radius of Nd3+ ions transported on by the replacement of Zn2+ by Nd3+ during the doping process.

Table 1: X-ray diffraction parameter values of the ZnO and Nd^{3+} doped ZnO NPs

Samples	Lattice parameter values (nm)		Atomic packing factor (c/a)	Volume (V) $(Å)^3$	Cos φ	Position parameter (u)	Bond Length (Zn-O) L (Å)	Average crystallite size D (nm)
	a	c						
ZnO NPs	3.2506	5.2007	1.5999	47.590	0.9464	0.3802	1.5549	49

Nd^{3+} doped ZnO NPs	3.2486	5.1938	1.5987	47.468	0.9464	0.3804	1.5548	42

3.2. Structural analysis

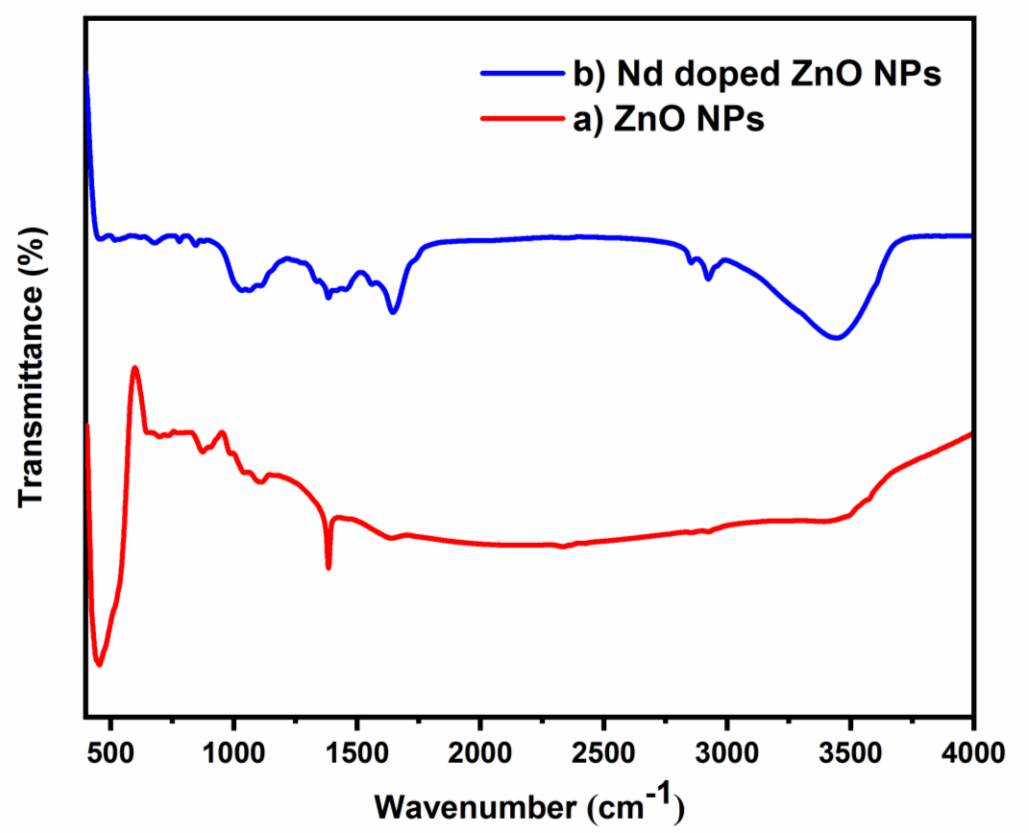

Fig. 3. FT-IR spectra of a) ZnO NPs b) Nd^{3+} doped ZnO NPs

The well-defined peaks at 3441, 1684, 873, and 465 cm^{-1} are part of the FTIR spectra displayed in Fig.3. The absorption peaks are noted at 3441 and 1684 cm^{-1} due to the stretching vibration of the O-H band [20, 21]. The peak observed at 465 cm^{-1} related to Zn-O stretching vibration in ZnO matrix [22]. The absence of any additional absorption bands in the FTIR spectrum indicates that the manufactured NPs are nearly pure and devoid of any obvious impurities. The vibration mode at 445 cm^{-1} in Nd^{3+} doped ZnO samples exhibits the Zn-Nd-O stretching band and may be generated by Nd^{3+} ions replacing Zn^{2+} sites [23]. Additionally, this peak related with a reduction in Nd^{3+} concentration validated the replacement of Nd^{3+} ions in the ZnO lattice.

3.3. Morphological analysis

Fig. 4 depicts the surface morphology of the ZnO and Nd^{3+} doped ZnO NPs created using *H. indicus* root extracts. The hexagonal and flake-like nanostructures in ZnO and Nd^{3+} doped ZnO NPs, respectively, were seen in the FESEM images. For ZnO and Nd^{3+} doped ZnO NPs, the average particle sizes were calculated to be 49 and 42 nm from XRD analysis. The nucleation and subsequent growth rates of ZnO NPs are slowed down by the rare earth metal ions, which reduces the thickness of the NPs.

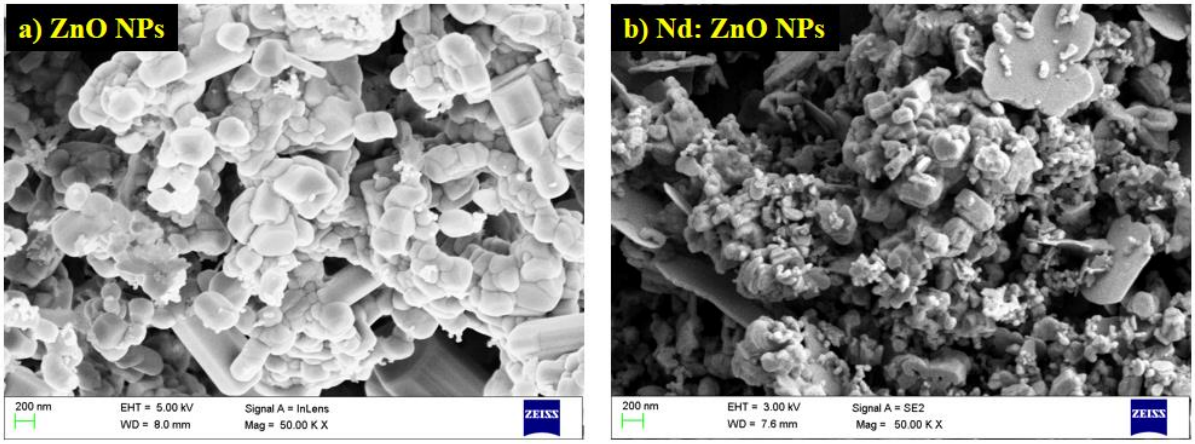

Fig. 4. FE-SEM images of a) ZnO NPs b) Nd^{3+} doped ZnO NPs

3.4. Compositional analysis

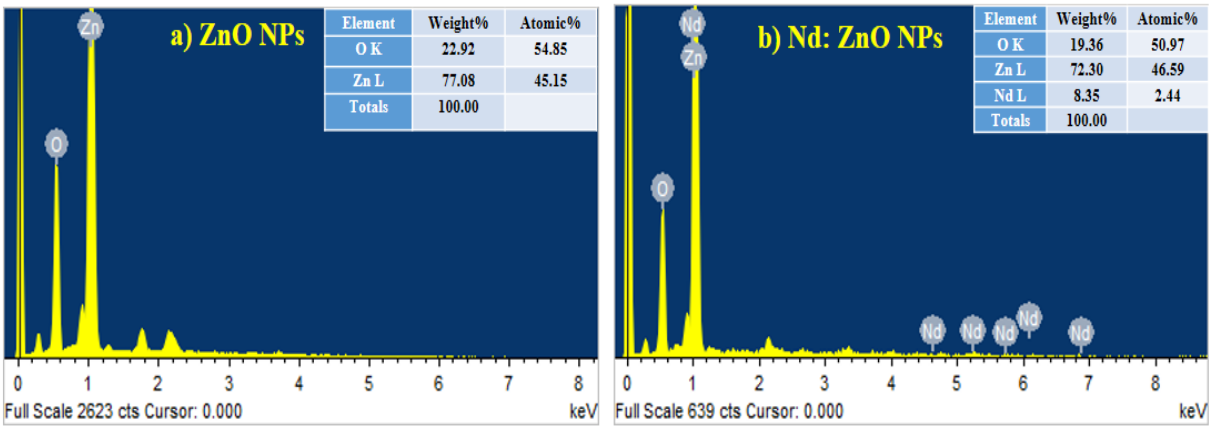

Fig. 5. EDAX spectra of a) ZnO NPs b) Nd^{3+} doped ZnO NPs

EDAX was used to analyze the elemental properties of the ZnO and Nd^{3+} doped ZnO NPs produced from *H. indicus* root extracts. Fig. 5 displays the EDAX images of ZnO and Nd^{3+} doped ZnO NPs. The Zn and O elements are present in the ZnO matrix with the composition of 22.92% and 77.08%. The Zn, O and Nd were detected in the sample for Nd^{3+} doped ZnO NPs. This could be Nd^{3+} ions integrated into the ZnO matrix.

3.5. Optical absorption studies

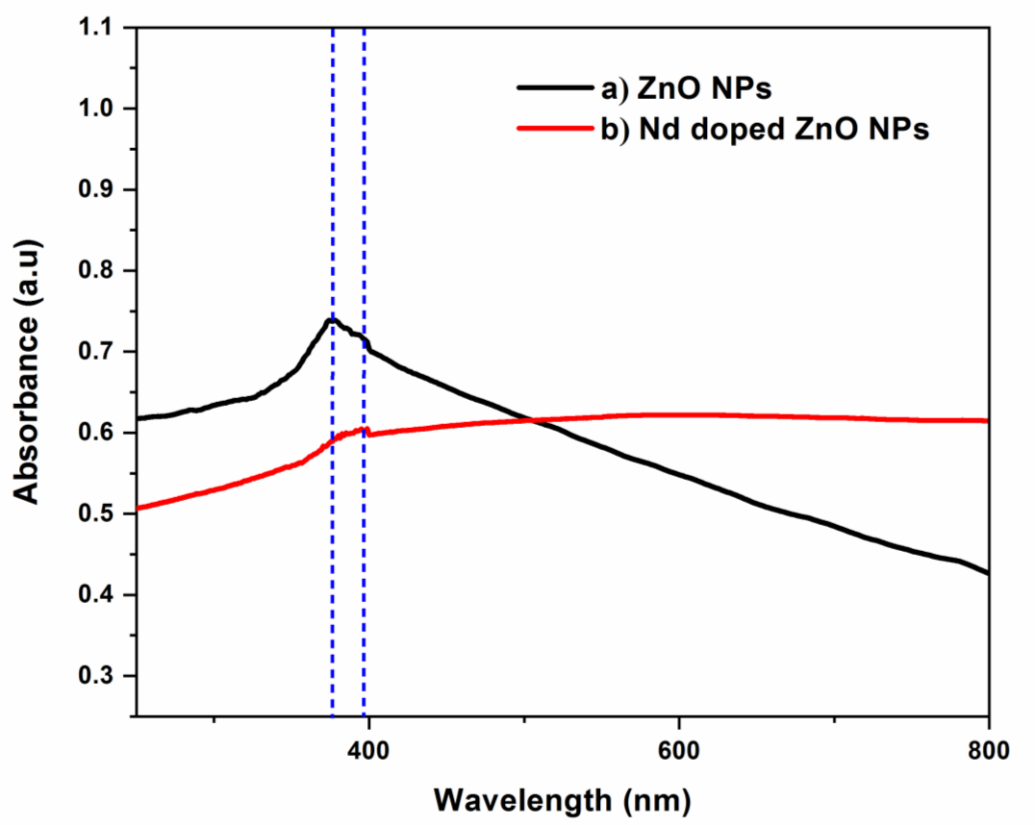

Fig. 6. UV-vis spectrum of a) ZnO NPs b) Nd^{3+} doped ZnO NPs

Figure 6 displayed the UV-vis spectrum in the range of 350–800 nm. he as-prepared NPs were evenly dispersed in distilled water and then ultrasonified for 15 minutes before UV-Vis spectra were collected. The absorption peaks for ZnO NPs and ZnO NPs doped with Nd3+ can be

observed at 374 nm and 395 nm, respectively, as a consequence of the photoexcitation of electrons from the valence band to the conduction band. [24]

3.6. Antimicrobial Activity:

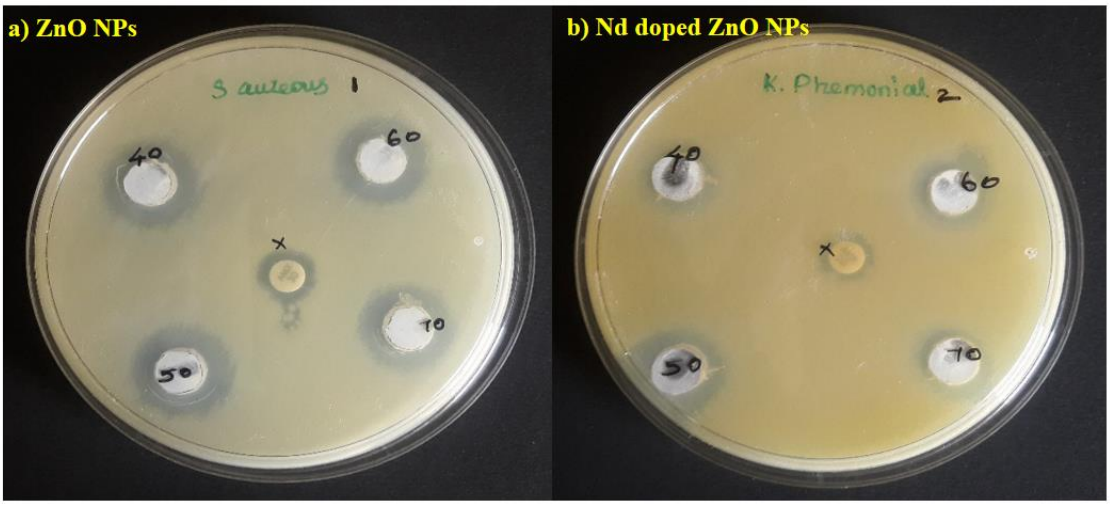

Fig. 7. Zone of inhibition of a) ZnO NPs and b) Nd^{3+} doped ZnO NPs against *S. aureus* and *K. phnemonea*

Fig.7 illustrations the antibacterial activity of ZnO and Nd^{3+} doped ZnO NPs at a concentration of 1.5 mg/ml. The antibacterial effect of Nd^{3+} doped ZnO NPs is greater than that of ZnO NPs, according to this study. Table 1 shows the values for antibacterial activity.

In view of the findings, the zones were enhanced in a direct relationship with the quantity of Nd3+ ion dopant used to treat the investigated bacteria. Due to variations in cell wall composition and structure, the inhibitory zone of G- bacteria is larger than that of G+ bacteria. The mechanism of as-prepared NPs with antibacterial activity is depicted in Figure 8.

The prepared NPs had particle sizes of 41 and 36 nm for ZnO and Nd^{3+} doped ZnO, respectively, according to XRD data. The Nd^{3+} doped ZnO NPs showed a crystallite size of 36 nm, which is associated with increased antibacterial activity. In antibacterial testing, it was shown that manufactured NPs with irregular surfaces and sharp edges link to the bacterial wall and destroy the cell membrane [25].

The FESEM image clearly displays diverse morphologies for ZnO and Nd^{3+} doped ZnO NPs, such as hexagonal and flake structures. Antibacterial activity was observed on the outer ridges of the Nd3+ doped ZnO NPs but not on the flat surfaces of other NPs, revealing

that antibacterial activity is substantially greater potent on surfaces with uneven ridges. [24]. Photoluminescence investigations indicated that increasing Nd^{3+} doping in ZnO NPs causes more faults (PL). The PL investigation of Nd^{3+} doped ZnO NPs reveals that when the oxygen vacancies develop in response to dopant, green emission increases [26].

We find that Nd^{3+} doped ZnO NPs are a more effective antibacterial agent than ZnO NPs based on antibacterial tests. According to the comparative statement, the current investigation has verified that both ZnO and Nd3+ doped ZnO, exhibit weak antibacterial activity. It's crucial to remember that each sample had potent antibacterial activity against both G+ and G- bacteria.

Table: 1 Antimicrobial activities of the as-prepared materials for against human pathogens

S. No	Concentration of ZnO and Nd^{3+}doped ZnO NPs (µL)	Zone of inhibition (mm)	
		Gram positive strains (ZnO NPs)	Gram negative strains (Nd^{3+} doped ZnO NPs
		S. aureus	*K. pneumonia*
1	40	1.4	1.8
2	50	1.5	1.7
3	60	1.3	1.5
4	70	1.4	1.6

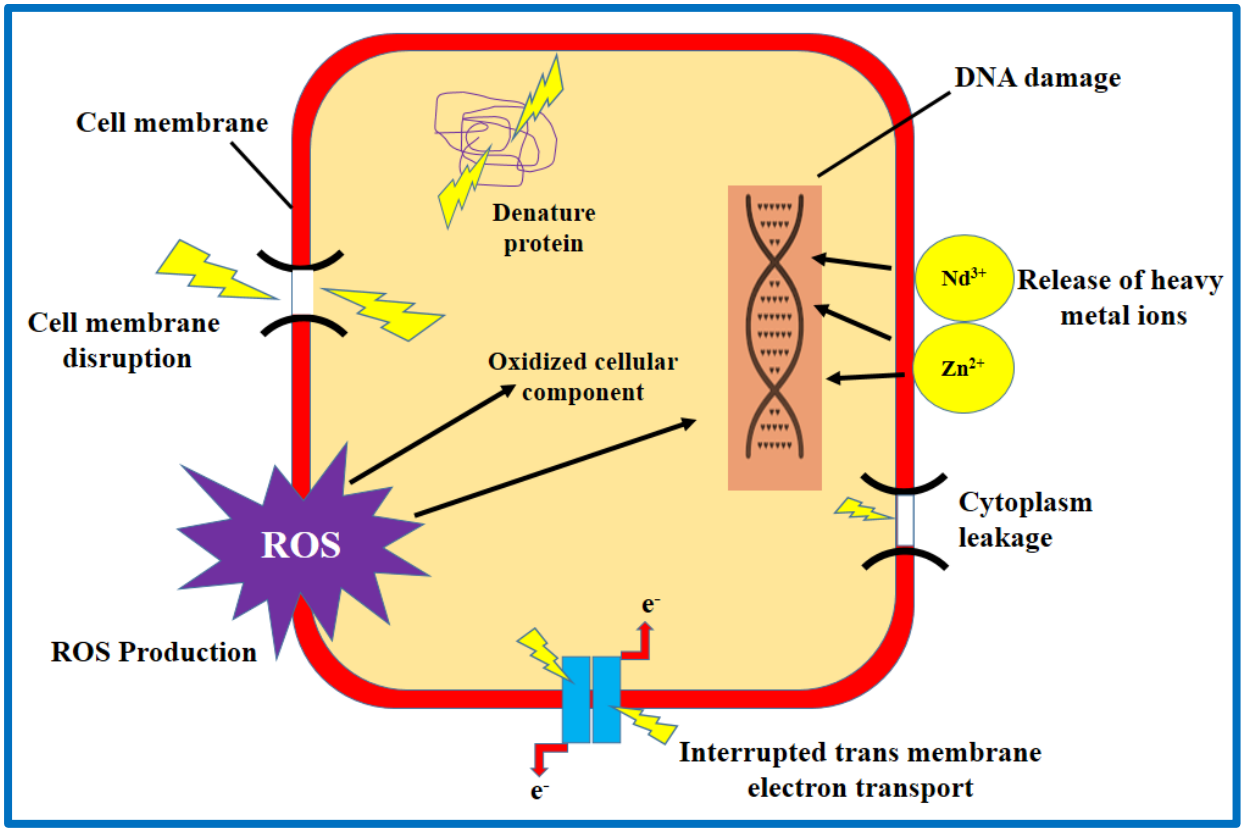

Fig. 8. Antimicrobial mechanism of the as-prepared material against bacterial pathogens

4. Conclusion

In summary, the use of root extracts from *H. indicus*, ZnO and Nd^{3+} doped ZnO NPs were effectively synthesized via simple precipitation route. Using XRD study, the hexagonal structure of as-prepared sample was determined. This study also demonstrated that Nd^{3+} ions have replaced Zn^{2+} ions in the ZnO matrix's lattice location. In this investigation, the Zn^{2+} site was found to be occupied by Nd^{3+} ions, and FTIR analysis was used to validate that all functional groups were present. For ZnO and Nd^{3+} doped ZnO NPs seen through FESEM, hexagonal and flake-like morphologies were identified. The G+ and G- bacterial strains were used in the antibacterial experiments. In order to account for the oxygen vacancies linked to the electron-hole pairs of the NPs, it was discovered that the higher concentration of Nd^{3+} doped ZnO NPs had a stronger antibacterial impact than the lower concentration of Nd^{3+}.

5. References:

[1]. Albrecht M.A., Evan C.W., Raston C.L. (2006) Green chemistry and the health implications of nanoparticles. Green Chem., 8, 417–432. https://doi.org/10.1039/B517131H

[2]. Rao A. N., Sivasankar B., Sadasivam V. (2009) Kinetic study on the photocatalytic degradation of salicylic acid using ZnO catalyst. J. Haz. Mat., 166, 1357–1361. https://doi.org/10.1016/j.jhazmat.2008.12.051

[3]. Sunandan B. K., Samir P., Joydeep D. (2012) Nanostructured Zinc Oxide for water treatment. Nanosci. Nanotech., 2, 90.

[4]. Dhermendre K., Tiwari J., Behari J., Prasenjit S. (2008) Application of nanoparticles in waste water treatment. World appl. Sc. J., 3(3), 417-433.

[5]. Rajendran R., Balakumar C., Hasabo A., Mohammed A., Jayakumar S., Vaideki K., Rajesh E. M. (2010) Use of zinc oxide nano particles for production of antimicrobial textiles. Int. J. Eng. Sc. Tech., 2(1), 202-208. DOI: 10.4314/ijest.v2i1.59113

[6]. Zhang L., Jiang Y., Ding Y., Daskalakis N., Jeuken L., Povey M., Alex J., Neill O., York D. W. (2010) Mechanistic investigation into antimicrobial behaviour of suspensions of ZnO nanoparticles against *E. coli*. J. Nanoparticle Res., 12, 1625–1636. https://doi.org/10.1007/s11051-009-9711-1

[7]. Ferracane J., Jack L. (2001) Materials in Dentistry: Principles and Applications, Lippincott Williams and Wilkins.

[8]. Richard V. N. (2002) Introduction to Dental Materials, 2nd ed. Elsevier Health Sciences.

[9]. Gnnasangeetha D., Sarala T. D. (2013) Biogenic production of zinc oxide nanoparticles using *Acalypha indica*. J. Chem. Bio Phy Sci., 4(1), 238-246.

[10]. Sangeetha G., Rajeshwari S., Venckatesh R. (2011) Green synthesis of zinc oxide nanoparticles by *Aloe barbadensis* miller leaf extract: structure and optical properties. Mater. Res. Bull., 46, 2560–2566. 10.1016/j.materresbull.2011.07.046

[11]. Shekhawat M. S., Manokari M. (2014) Biogenesis of zinc oxide nanoparticles using *Morinda pubescens* J.E. Smith extracts and their characterization. Int. J. Bioeng. Tech., 5(1), 1-6.

[12]. Shekhawat M. S., Ravindran C. P., Manokari M. (2014) Biosynthesis of zinc oxide nanoparticles from *Passiflora foetida* L. extracts and their characterization. Int. J. Green and Herbal Chem., 3(2), 518-523.

[13]. Shekhawat M. S., Ravindran C. P., Manokari M. (2014) A biomimetic approach towards synthesis of zinc oxide nanoparticles using *Hybanthus enneaspermus* (L.) F. Muell. Trop. Plant Res., 1(2), 55-59.

[14]. Shekhawat M. S., Ravindran C. P., Manokari M. (2015) A green approach to synthesize the zinc oxide nanoparticles using aqueous extracts of *Ficus benghalensis* L. Int. J. BioSci. Agri. Tech., 6(1), 1-5.

[15]. Shekhawat M. S., Ravindran C. P., Manokari M. (2015) An ecofriendly method for the synthesis of zinc oxide nanoparticles using *Lawsonia inermis* L. aqueous extracts. Int. J. Innov., 5(1), 1-4.

[16]. Nadkarni A. N. (1989) Indian Materia Medica, Vol I. Popular Book Depot, Bombay, pp. 619.

[17]. Austin A. (2008) A review on Indian Sarasaparilla, *Hemidesmus indicus* (L.) R. Br. J. Biol. Sci., 8(1), 1-12. DOI: 10.3923/jbs.2008.1.12

[18]. Nagarajan S., Rao J. M., Gurudutt K. N. (2001) Chemical composition of the volatiles of *Hemidesmus indicus* R. Br. Flav. Frag., 1 (3), 212-214. https://doi.org/10.1002/ffj.985

[19]. Zhang Y, Shi E. W, Chen Z. Z. (2010) Magnetic properties of different temperature treated Co- and Ni-doped ZnO hollow nanospheres. Mater. Sci. Semicond. Process., 13(3), 132-136. https://doi.org/10.1016/j.mssp.2010.05.002

[20]. Wang Y., Liao X., Huang Z., Yin G., Gu J., Yao Y. (2010) Physicochemical and Engineering Aspects. Colloids Surf A., 372, 165–171.

[21]. Hlaing Oo W.M., Mc Cluskey M.D., Lalonde A.D., Norton M.G. (2005) Infrared spectroscopy of ZnO nanoparticles containing CO_2 impurities. Appl. Phys. Lett., 86, 73111. https://doi.org/10.1063/1.1866511

[22]. Yayapao O., Thongtem T., Phuruangrat A., Thongtem S. (2013) Ultrasonic-assisted synthesis of Nd-doped ZnO for photocatalysis. Mater. Lett., 90, 83–86. DOI: 10.1016/j.matlet.2012.09.027

[23]. Ghosh M., Dilawar N., Bandyopadhyay A.K., Raychaudhuri A.K. (2009) Phonon dynamics of Zn(Mg,Cd)O alloy nanostructures and their phase segregation. J. Appl. Phys., 106, 84306. https://doi.org/10.1063/1.3243341

[24]. Liu M., Kitai A.H., Mascher P. (1992) Point defects and luminescence centres in zinc oxide and zinc oxide doped with manganese. J. Lumin., 54(1), 35-42. https://doi.org/10.1016/0022-2313(92)90047-D

[25]. Karthikeyan M, Jafar Ahamed A, Karthikeyan C, Vijaya Kumar P. (2019) Enhancement of antibacterial and anticancer properties of pure and REM doped ZnO nanoparticles synthesized using *Gymnema sylvestre* leaves extract. SN Applied Sciences., 1, 355. https://doi.org/10.1007/s42452-019-0375-x

[26]. Vijayaprasath G, Murugana R, Palanisamy S, Prabhu N.M, Mahalingam T, Hayakawa Y, Ravi G. (2016) Role of nickel doping on structural, optical, magnetic properties and antibacterial activity of ZnO nanoparticles. Materials Research Bulletin., 76, 48-61. https://doi.org/10.1016/j.materresbull.2015.11.053